Supplementary Information

Design of blueberry anthocyanins/TiO$_2$ composite layer-based photoanode and N-doped porous blueberry-derived carbon-loaded Ni nanoparticles-based counter electrode for dye-sensitized solar cells

Xiang Qin[1,2#]• Jingjing Liu[1,2#]• Genhui Teng[1,2]• Baorui Liu[1,2]• Yanhui_Xie[1,2]• Lin Ma[1,2]• Dongying Hu[1,2]*

[1] School of Resources, Environment and Materials, Guangxi University, Nanning, 530004, China.

[2] State Key Laboratory of Featured Metal Materials and Life-cycle Safety for Composite Structures, Guangxi University, Nanning, 530004, China.

[#] Xiang Qin and Jingjing Liu contributed equally to this work.

* Corresponding author (Dongying Hu). Tel: +86-771-3232200.

E-mail address: hdy@gxu.edu.cn   hdygxu@163.com (Dongying Hu) *

Qinxiang542968@163.com (Xiang Qin)

wxxxljj@163.com (Jingjing Liu)

1829380331@qq.com (Genhui Teng)

785631176@qq.com (Baorui Liu)

3039215046@qq.com (Yanhui Xie)

1319548675@qq.com (Lin Ma)

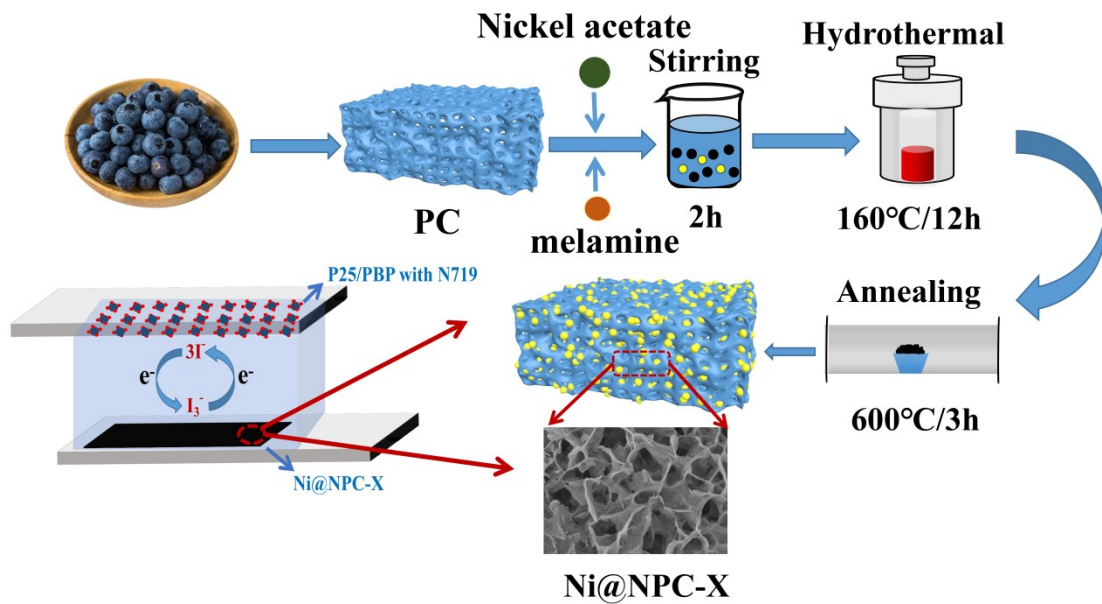Fig.S1 Schematic diagram of the preparation of Ni@NPC-X composite materials

Fig.S2. N$_2$ adsorption-desorption isotherms of P25 and P25/PBP (a), pore size distribution plots (b)

Fig.S3 SEM images of Ni@NPC-1 (a-c), Ni@NPC-1.5 (d-f), Ni@NPC-2 (g-i)

Fig.S4 N_2 adsorption-desorption isotherms of PC (a), Ni@PC (b), Ni@NPC-1 (c),

Ni@NPC-1.5 (d), Ni@NPC-2 (e)

Fig.S5 FT-IR spectra (a) and UV-vis absorption spectra (b) of samples, the inset in (b)

is general structure of anthocyanin

Fig.S6 Photocurrent density voltage (J-V) curves (a), CV curves (b), Nyquist plots of

the assembled DSSCs by P25/PBP photoanode and Ni CEs

Fig.S7 Tafel curves of the symmetrical cells based on different CEs

1 Experimental sections

1.1 The preparation of photoanode materials

Fig.S1 Schematic diagram of the preparation of Ni@NPC-X composite materials

1.2 Characterization

An X-ray diffractometer (XRD, DX-2700A, Dandong Haoyuan Instrument Co., Ltd., China) was used to obtain the XRD patterns. Scanning electron microscope (FE-SEM, Zeiss Sigma 300, Germany) was used to measure the morphology. X-ray photoelectron spectrometer (XPS, Thermo Fisher Scientific K-Alpha Plus) records the

distribution of elements. Fourier transform infrared (FTIR) spectra were obtained using a Nicolet iS 50 spectrophotometer (Thermo Fisher Scientific, USA). Raman spectroscopy (inVia Reflex, Renishaw, UK) is measured at 532 nm. The Brunauer-Emmett-Teller (BET, JW-BK400, Jingwei Gaobo Co., Ltd. China) was used to test the specific surface area and pore size distribution.

The photocurrent density voltage (J-V) curve of DSSCs was tested by a digital source meter (Keithley 2450) under simulated AM 1.5G illumination (100 mW /cm^2) with 0.25 cm^2. The electrochemical performance was tested by an electrochemical workstation (CS350, Wuhan Corrtest Instruments Corp., Ltd, China). The electrochemical impedance spectroscopy (EIS) of symmetrical cells was measured in a frequency range of 0.1-100 kHz and at 10 mV. The Tafel polarization was carried out at a holding voltage range of -0.6V to 0.6V and at 50 mV/s. Cyclic voltammetry (CV) curves were determined in a three electrode system with electrolyte containing 0.001 M I$_2$, 0.01 M LiI and 0.1 M LiClO$_4$ in acetonitrile solution at 50 mV/s, in which CE is the working electrode, Pt wire is the auxiliary electrode, the Ag/Ag$^+$ as the reference electrode. The open circuit voltage decay curve (OCVD) can be determined through turning off the light source after 10s of illumination.

2 Results and Discussion
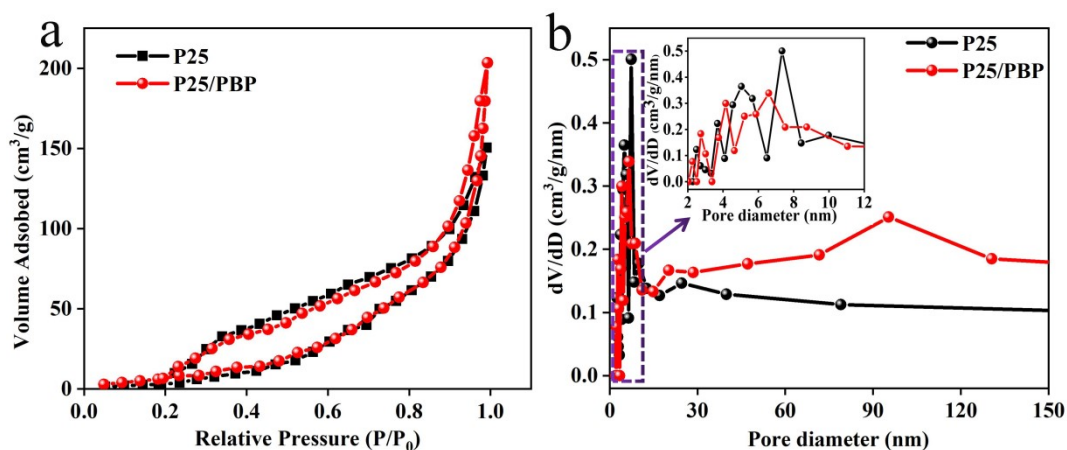
Fig.S2. N$_2$ adsorption-desorption isotherms of P25 and P25/PBP (a), pore size distribution plots (b)

It is easy to see that the carbon substrate has an irregular shape when the N-doped is 1 g or 2 g. As shown in Fig.S3(a-c), when the N-doped amount X=1 g, the petal-like structure of the Ni@NPC-1 carbon substrate is not fully formed, and the pore structure is small, which leads to agglomeration of loaded Ni nanoparticles. In addition, it can also be found that the carbon based material structure was destroyed when excessive amounts of melamine were added. As shown in Fig.S3(g-i), the petal-like structure of the Ni@NPC-2 carbon based material breaks down and causes blockage of the pore structure. In Fig.S3(d-f), the petal-like structure formed by the Ni@NPC-1.5 composite material enables the uniform loading of Ni nanoparticles, which is very important for the electrocatalytic performance of the material. The structural characteristics of the Ni@NPC-X composite material show that the morphology of the composite material can be adjusted by reasonably controlling the N-doped content.
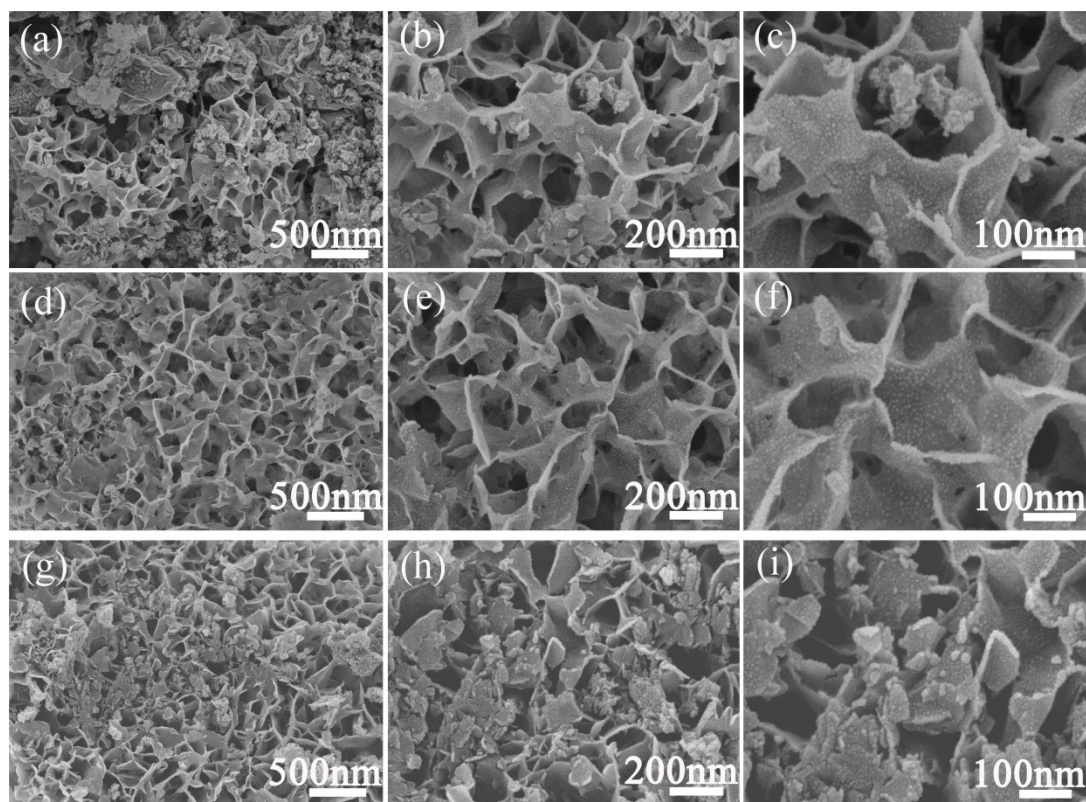

Fig.S3 SEM images of Ni@NPC-1 (a-c), Ni@NPC-1.5 (d-f), Ni@NPC-2 (g-i)

The pore characteristics of PC, Ni@PC, Ni@NPC-1, Ni@NPC-1.5 and Ni@NPC-2

were studied by N_2 adsorption-desorption isotherms, as shown in Fig.S4.The N_2 adsorption isotherm of all samples is roughly expressed as a comprehensive I/IV isotherm, including the micropore filling in the relatively low pressure (P/P_0) area and the hysteresis loop in the relatively low and high pressure P/P_0 (0.4-1) area, indicating that all samples have a microporous/mesoporous hybrid structure. When the relative pressure (P/P_0) is less than 0.1, N_2 absorption is very obvious, indicating that there are micropores in the sample. The IV-type isotherm and the H_2-type hysteresis loop appear in the relative pressure (P/P_0) within the range of 0.4-1, which verifies the existence of mesopores in the sample. According to the calculation of the Barrett-Joyner-Halenda (BJH) pore size distribution, the average pore size of all samples is about 2.3nm. Before being undoped with N, the specific surface area of PC is 871.6 m^2/g, which is greater than the 599.5 m^2/g of Ni@PC. This is because Ni nanoparticles loaded on the carbon-based material cover part of the voids. With the increase of N doping content, the specific surface area of Ni@NPC-X first increases and then decreases, from 777.8 m^2/g of Ni@NPC-1 to 1185.7 m^2/g of Ni@NPC-1.5, and then decreases to 189.7 m^2/g of Ni @NPC-2. After the addition of heteroatom N, the structure of the carbon-based material changes and the specific surface area increases. When the N content is too much, the structure of the carbon-based material is destroyed, and the specific surface area is reduced, which also can be observed by the up analysis of SEM morphology characteristics. Carbon-based materials with a large specific surface area can provide a large number of active sites, increase the contact and penetration area between the electrolytes of the material, and improve the electrochemical performance of CE.
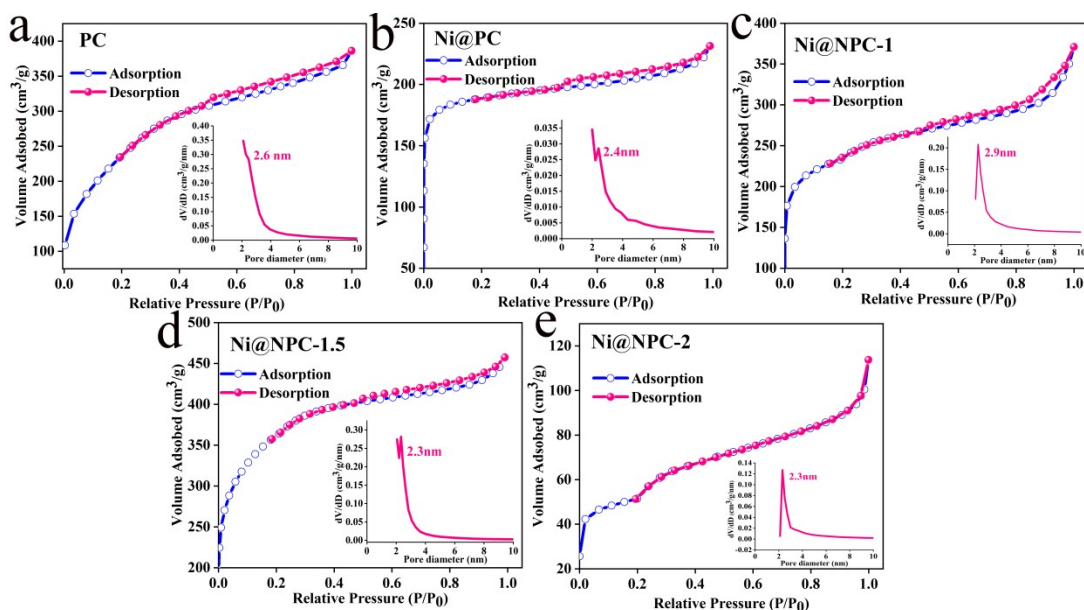
Fig.S4. N$_2$ adsorption-desorption isotherms of PC (a),Ni@PC (b),Ni@NPC-1 (c), Ni@NPC-1.5 (d), Ni@NPC-2 (e)

Fig.S5a shows the FT-IR spectra of P25, PBP and P25/PBP. For P25, the broad vibrational band appearing in the range 500-700 cm^{-1} is the characteristic TiO$_2$ absorption band, the vibration peak at 2300 cm^{-1} is attributed to Ti-O stretching vibration of TiO$_2$, and the vibration peak at 3450 cm^{-1} is attributed to the stretching vibration of hydroxyl group, which is mainly due to the chemical and physical absorption of H$_2$O molecules on the surface of the material. For PBP, the peaks at 3450, 2934, 1721, 1630, 1068 and 1110 cm^{-1} represent -OH, -CH, C=O, C=C, ester linkage and C-O groups, respectively. [1] These results prove the existence of functional groups of anthocyanin in PBP. [1] On the other hand, after PBP was calcined at 450℃, the generation of oxygen-containing groups at 3450, 1630 and 1110 cm^{-1}, proved to be -OH, C=C and C-O groups [2], which confirmed that PBP after calcination without any impurities, which is consistent with XRD. In addition, the lower intensity of the FT-IR spectrum of P25/PBP before calcinationis caused by the physical and chemical interaction between the anthocyanin molecules in the PBP and the TiO$_2$ nanoparticles. In the FT-IR spectrum of P25/PBP after being calcined at 450℃, the stretching vibration of Ti-O at 2350 cm^{-1} is more obvious, indicating that the crystallinity of

1 TiO$_2$ is better after heat treatment. There are functional groups of TiO$_2$ and carbon

2 atoms at the same time, which further shows that P25/PBP is composed of TiO$_2$ and

3 carbon atoms.

4 In order to analyze the effect of adding PBP on the light absorption of P25, the UV

5 absorption spectra were tested. Fig.S5b shows the absorption spectra of P25, P25/PBP

6 and PBP dyes at a wavelength of 300~800 nm. It can be seen that all samples have

7 light absorption between 300-800 nm. PBP dye solution has a strong absorption peak

8 at 538nm, which is a characteristic peak of anthocyanins [3], indicating that PBP dye

9 contains anthocyanins, which is consistent with the FT-IR results. Different from the

10 absorption peak of PBP dye solution, the absorption peak of P25/PBP is red-shifted

11 and the absorption intensity is broadened. This is because the carbonyl and hydroxyl

12 groups in anthocyanins combine with Ti-O, which enhances the conjugation effect

13 and reduces the energy level of the dye. [4]

14
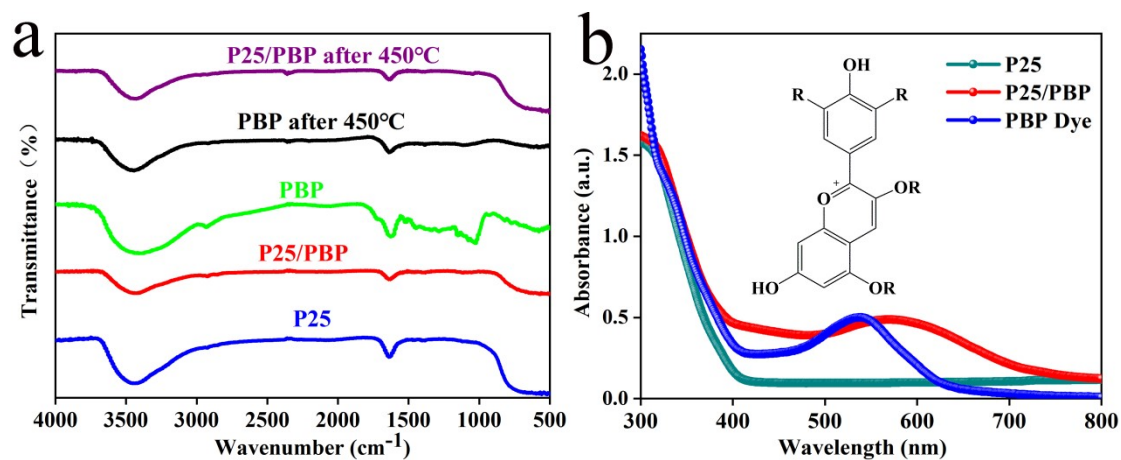
15 Fig.S5 FT-IR spectra (a) and UV-vis absorption spectra (b) of samples; the inset in (b) is general

16 structure of anthocyanin

17
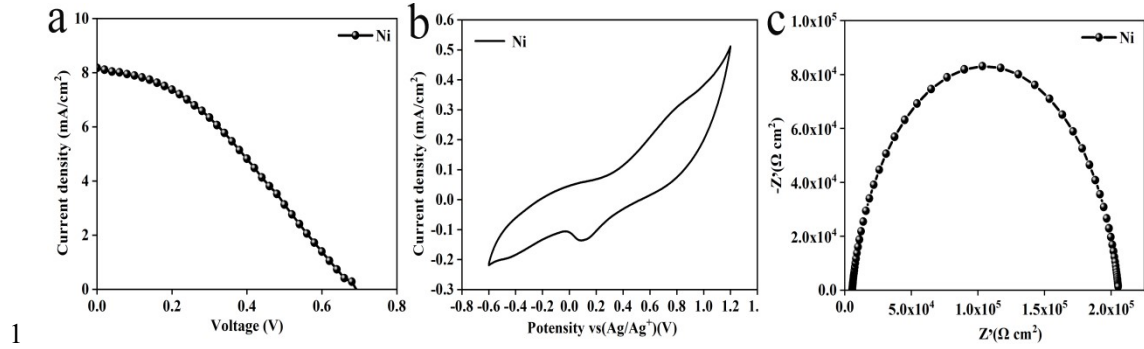
1

2 Fig.S6 Photocurrent density voltage (J-V) curves (a), CV curves (b), Nyquist plots of the

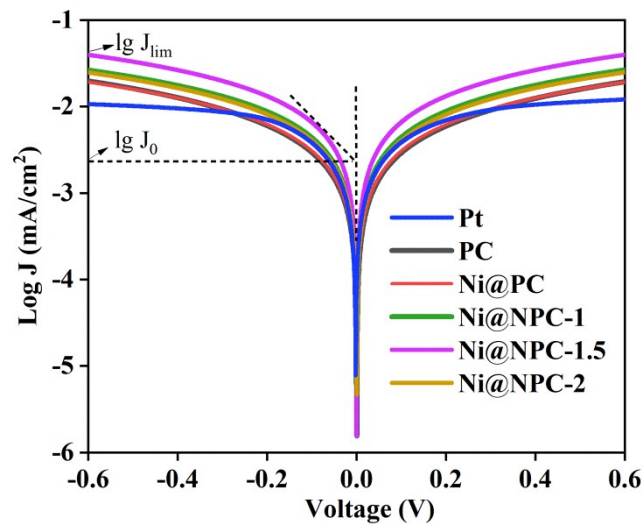3 assembled DSSCs by P25/PBP photoanode and Ni CEs.

4

5 **Table S1**

6 The electrochemical characterization of pure Ni

CEs	V_{ov}	J_{sc}	FF	PCE	E_p	I_p	R_{ct}	R_s
	(V)	(mA/cm^2)		(%)	(mV)	(mA/cm^2)	(Ω cm^2)	(Ω cm^2)
Ni	0.69±0.01	8.18±0.2	0.35±0.01	1.98±0.02	794	-0.135	1.99×10^5	0.55×10^5

7

8

9 Fig.S7 Tafel curves of the symmetrical cells based on different CEs.

10

11 **References**

12 1. I.C. Maurya, P. Srivastava, L. Bahadur, *Opt. Mater.,* 2016, **52**, 150-156.

13 2. P. Xue, Y. Bao, Q. Li, C. Wu, *Phys. Chem. Chem. Phys.,* 2010, **12**, 11342-11350.

14 3. L. Longo, G. Vasapollo, *Food Chem.,* 2006, **94**, 226-231.

1   4. S.S. Soni, K.B. Fadadu, J.V. Vaghasiya, B.G. Solanki, K.K. Sonigara, A. Singh, D. Das, P.K.

2   Iyer, *J. Mater. Chem. A*, 2015, **3**, 21664-21671.

3